Nanofiltration Theory: An Analytic Approach for Single Salts

Xavier Lefebvre, John Palmeri,* and Patrice David

Institut Européen des Membranes (CNRS ENSCM UMR 5635), Université Montpellier II, CC047, Place Eugène Bataillon 34095 Montpellier Cedex 5, France

Received: March 29, 2004; In Final Form: August 17, 2004

We determine the complete set of nanofiltration (NF) parameters (rejection rate, electric filtration potential, volume flux density) of single salts using an analytical approach. Our model is based on the hindered extended Nernst−Planck (ENP) and Stokes equations. We solve the transport equations within the scope of the hindered electrotransport (HET) model, which takes into account ion charge and size (rejection is controlled by both electrostatic and steric effects). We also validate these calculations using both an analytical solution to the classic ENP model, which neglects the ion size, and numerical methods via our NF simulation program, Nanoflux. A preliminary application of the model to organic membranes suggests that the HET model provides a coherent description of ion transport in charged nanoporous membranes.

1. Introduction

Understanding nanofiltration (NF) transport mechanisms is essential for making progress in optimizing membrane separation technology.[1−3] Despite recent advances, this technique presents a number of difficulties for implementation in industrial processes. The complexity of the transfer mechanisms makes the prediction of membrane performance extremely difficult in charged nanoporous membranes. Indeed, the pore-level description in charged porous media is usually provided by the space-charge model (SCM).[4−10] Recent work employing sophisticated statistical mechanical methods suggests that this model, or suitable extensions thereof, should also be valid in nanopores (perhaps in part because of a canceling out of effects not taken into account in this simplified model).[11,12] In the case of sufficiently weak membrane charge and tight pores, the SCM can be approximated by a homogeneous electrotransport model comprising the mesoscopic extended Nernst−Planck (ENP) equations and local charge electroneutrality.[13−19] The mesoscopic homogeneous model can be obtained from the pore-level SCM using 3-D volume-averaging techniques that do not require a simple capillary structure at the pore level and are therefore useful even for nanofilters exhibiting complicated morphologies. A computer simulation program, Nanoflux, has been developed in our laboratory to solve the homogeneous electrotransport model for up to 11 ionic species using numerical methods.[16] To gain a deeper understanding of NF transport and validate Nanoflux numerical calculations, an analytical approach appeared to be essential.[15,17−19]

Because of its complexity, the more detailed type of microscopic modeling currently being employed to understand transport in the short ion channels (∼5 nm in length) of cell membranes has not yet been applied to the thicker (∼1 μm) and morphologically more complex artificial NF membranes. A major challenge in the field of NF has been extracting useful physical predictions from the highly nonlinear set of coupled flow and transport equations. By attempting to find an appropriate compromise between the microscopic realism of a model and its tractability, this is the main goal of the present work.

* Corresponding author. E-mail: John.Palmeri@iemm.univ-montp2.fr. Tel.: +33 4 67 14 91 30.

We demonstrate here that, for a single salt, an analytical solution in the form of parametrized equations can be obtained for all physical NF parameters. (The complexity of an analytical solution is such that it seems possible to treat only one salt.) We study not only ionic rejection (as is often the case in recent NF modeling), but also the electric filtration potential and transmembrane volume flux density. An innovative feature of this work is the analytical determination of ion partition coefficients within the scope of a generalized model that can easily accommodate other forces (steric, dielectric, Born solvation, etc.), in addition to electrostatic (Donnan), acting at the external solution−membrane interfaces. The hindered electrotransport (HET) theory, in which only the electrostatic and hindered transport effects are taken into account, is a special case of this more general model. Although the analytical calculations presented here are illustrated via specific examples using the simpler HET model, other interfacial forces can easily be included.

Within the scope of the ENP model,[6,20] NF parameters have been calculated analytically only for [1:1] salts[13,14,21] or in limiting cases (high membrane charge density[22] or high volume flux, for instance[15]); within the scope of the HET model, analytic rejection results exist only for [1:1] salts.[23]

This paper is organized as follows: We start in section 2 with a short presentation of the models used in this work. We continue in section 3 with the determination of the ion partition coefficients in the HET model. In section 4, we solve both the hindered and the classic ENP equations in order to find an analytic function representing the rejection rate as a function of the Péclet number (which is proportional to the volume flux density j_v). We then calculate, in sections 5 and 6, the electric filtration potential by using the vanishing of the electric current density in NF and obtain the volume flux density (osmotic and electroviscous effects) by solving the averaged Stokes equation. To validate these analytical calculations, we compare them with numerical results obtained using Nanoflux and with the results of simplified equations based on limiting cases. To provide a preliminary experimental test of the global coherence of the HET model, we also present in section 7 an application to organic membranes. We show that the experimental rejection and filtration potential can be well reproduced by using a unique

10.1021/jp048631t CCC: $27.50
Published on Web 10/07/2004

choice for membrane pore size, charge density, and effective thickness in the model calculations.

2. Transport Models

We study the pressure-driven transport of ions across a nanoporous membrane separating a feed from a permeate compartment under open electrical circuit conditions. For simplicity, we neglect the effects of any supporting layers and concentration polarization (the influence of which can often be minimized by optimizing the operating conditions). Despite the extensive work on the modeling of solute transfer in NF over the past decade, a complete explanation of the basic mechanisms involved is still not available. In simple terms, the objective of any NF modeling study is to relate the incoming solute feed concentration, c_s^f, and imposed transmembrane pressure gradient, ΔP, to the outgoing solute permeate concentration, c_s^p, and volume flux density of the solution, j_v ($L \cdot h^{-1} \cdot m^{-2}$). The feed and permeate solute concentrations can be used to define the solute rejection, R, as

$$R = 1 - \frac{c_s^p}{c_s^f}$$

and the primary goal of the model is to predict R as a function of the volume flux density given the composition of the feed (ionic concentrations) and the properties of the membrane. A further goal is to predict the electric filtration potential across the membrane as a function of the volume flux density and the volume flux density as a function of ΔP. Here, we will be interested only in steady-state NF processes for which all quantities studied are independent of time and all fluxes are independent of position in the membrane.

The compositions of the feed and the permeate are determined by the concentration of each salt in the electrolyte mixture. Each salt is assumed to be completely dissociated into cations ($z_C > 0$) and anions ($z_A < 0$)

$$C_{\nu_{C,s}} A_{\nu_{A,s}} \rightarrow \nu_{C,s} C^{|z_c|+} + \nu_{A,s} A^{|z_A|-} \tag{1}$$

In the following, we work with only one salt (one anion and one cation).

Electroneutrality is respected in the system

$$z_1 c_1^f + z_2 c_2^f = 0 \qquad \text{(feed)} \tag{2}$$

$$z_1 c_1^p + z_2 c_2^p = 0 \qquad \text{(permeate)} \tag{3}$$

$$z_1 \bar{c}_1(x) + z_2 \bar{c}_2(x) + X_m = 0 \qquad \text{(membrane)} \tag{4}$$

where z_1 is the valence of the counterion (sign opposite that of the membrane charge), z_2 is the valence of the co-ion (same sign as the membrane charge), X_m is the constant membrane charge density (moles per liter of pore volume), $c_i^{f(p)}$ is the concentration of the ion i in the feed (f) or the permeate (p) (moles per liter), and $\bar{c}_i(x)$ is the average position-dependent concentration of ion i in the membrane (moles per liter of pore volume) ($0 \le x \le l_m$, where l_m is the thickness of the active layer of the membrane).

a. Classic Extended Nernst−Planck Equation. The ENP equation (eq 5) incorporates three contributions to the ion flux: a diffusive term, an electric migration term, and a convective term.[6] In the framework of the classic ENP model, the molar flux of ion i ($mol \cdot m^{-2} \cdot s^{-1}$) is given by

$$j_i = -\bar{D}_i \partial_x \bar{c}_i(x) - \frac{F}{RT} \bar{D}_i z_i \bar{c}_i(x) \partial_x \phi(x) + \bar{c}_i(x) j_v \tag{5}$$

where $\bar{D}_i$ is the effective ionic diffusion coefficient in the membrane ($m^2 \cdot s^{-1}$), $\phi(x)$ is the average electric potential (V), and j_v is the volume flux density ($m \cdot s^{-1}$ or $L \cdot h^{-1} \cdot m^{-2}$).

In this model, the transport is controlled only by electrostatic interactions acting on point ions, and therefore, the ratio $\bar{D}_i/D_i$ is a constant (independent of the ion) and $\bar{D}_i/D_i = l_m/l_{eff} = \varphi_p/\tau$, where τ is the tortuosity, φ_p is the porosity, and $l_{eff} = l_m \tau/\varphi_p$ is an effective membrane thickness.

Given that most of the transport resistance is to be found in the membrane, because of its large thickness compared to the Debye length and the relatively low fluxes, we have approximate thermodynamic and mechanical equilibrium across the membrane−external solution interfaces.[22] This approximate thermodynamic equilibrium can be obtained by first neglecting j_i and j_v in eq 5 and then integrating this equation across the membrane−external solution interfaces; this leads to constant (ideal) electrochemical potentials

$$\bar{\mu}_i(x) = RT \ln[\bar{c}_i(x)] + z_i F \phi(x) \tag{6}$$

across these interfaces.[22] At the interfaces (feed−membrane and membrane−permeate), this quasi-constancy leads to Donnan equilibrium

$$\begin{aligned} \mu_i^f &\approx \mu_i(0^+) \\ \mu_i^p &\approx \mu_i(l_m^-) \end{aligned} \tag{7}$$

where

$$\mu_i^{f(p)} = RT \ln(c_i^{f(p)}) + z_i F \phi^{f(p)} \tag{8}$$

is the "ideal" electrochemical potential of ion i in the feed (f) or permeate (p) and $x = 0^+$ and l_m^- are points just inside the membrane at the feed and permeate sides, respectively. The Donnan partition coefficients are then given by

$$k_i^f = \frac{\bar{c}_i(0^+)}{c_i^f} = \exp\left(-\frac{z_i F \Delta\phi_D^f}{RT}\right) \qquad \text{(feed)} \tag{9}$$

and

$$k_i^p = \frac{\bar{c}_i(l_m^-)}{c_i^p} = \exp\left(-\frac{z_i F \Delta\phi_D^p}{RT}\right) \qquad \text{(permeate)}$$

where $\Delta\phi_D^{f(p)}$ is the Donnan potential at the feed or permeate side

$$\Delta\phi_D^f = \phi(0^+) - \phi^f \quad \text{and} \quad \Delta\phi_D^p = \phi(l_m^-) - \phi^p$$

By combining eq 9 with electroneutrality (eq 4), an analytical solution for the ion partition coefficients can be found for symmetric salts and certain asymmetric ones ([1:2] and [2:1], for counter- and co-ion valences, respectively).[15]

b. General Hindered Extended Nernst−Planck Model. The classic ENP model assumes that only electrostatic effects control the transport of ions, which means that the pore radius should be much larger than the ionic radius. However, the loosest nanofiltration membranes contain pores of 1 nm in radius, which implies that this assumption is no longer valid. A coherent transport model has to account for ion size and perhaps other interactions not included in the classic ENP model. In such a

model, the bulk electrochemical potentials are given by

$$\mu_i^{f(p)} = RT \ln(\gamma_i^{f(p)} c_i^{f(p)}) + z_i F \phi^{f(p)}$$

where $\gamma_i^{f(p)}$ is the bulk activity coefficient that arises as a result of ion−ion interactions (taken to be unity in the classic ENP model). Moreover, the intramembrane electrochemical potentials contain an effective activity coefficient term, $\bar{\gamma}_i$, that accounts for all deviations from "nonideality" and thus encompasses contributions from the extra interactions, including the steric interaction, which depends on ion size

$$\bar{\mu}_i(x) = RT \ln[\bar{\gamma}_i(x)\, \bar{c}_i(x)] + z_i F \phi(x) \tag{10}$$

(in the interest of compactness we have included the so-called "standard chemical potentials" directly in the activity coefficients). By taking into account ion size and the other interactions, the classic ENP equations become the general hindered ENP expressions[24−26]

$$j_i = -\bar{D}_i \partial_x \bar{c}_i(x) - \frac{F}{RT} \bar{D}_i z_i \bar{c}_i(x) \partial_x \phi(x) + K_{i,c} \bar{c}_i(x) j_v - \bar{c}_i(x) \bar{D}_i \partial_x \ln(\bar{\gamma}_i) \tag{11}$$

where $\bar{D}_i = K_{i,d} D_i\ \phi_p/\tau = K_{i,d} D_i\ l_m/l_{eff}$ is the effective ion diffusivity in the membrane ($m^2 \cdot s^{-1}$), $K_{i,d}$ is the diffusive (steric/hydrodynamic) hindrance factor, and $K_{i,c}$ is the convective (steric/hydrodynamic) hindrance factor.

For the HET model, $\gamma_i^{f(p)} = 1$ and $\bar{\gamma}_i = (\Phi_i^S)^{-1}$, as only electrostatic and hindered transport effects are retained in the membrane. Here, Φ_i^S is the steric hindrance partition coefficient, defined as $\Phi_i^S = (1 - \lambda_i)^2$, where $\lambda_i = r_i/r_p$ with r_i and r_p the ion and the pore radii, respectively. Deen[27] has reviewed the different estimates for the hindrance factors, $K_{i,d}$ and $K_{i,c}$, for hard spheres in cylindrical pores and presented results that should be valid over the whole parameter range (see Appendix).

Unlike the ENP model, where the ratio $\bar{D}_i/D_i$ is constant, the HET model reveals that this ratio depends on the ionic species considered. Approximate interfacial thermodynamic equilibrium (eq 7) is also valid in this model, which gives rise to Donnan/steric partitioning across the external solution−membrane interfaces. We adopt the basic simplifying assumption that, within the membrane, the ions interact with each other and the membrane solely via the direct mean field electrostatic interactions, which implies inter alia that the cross-coupling terms that appear in more general theoretical frameworks (such as the Stefan−Maxwell approach) are negligible[6] and that the last term in the hindered ENP equation, involving the gradient of the effective activity coefficient, is also negligible in the core of the membrane. Note that this approximation does not require that all other ion−ion and ion−membrane interactions be weak *within* the core of the membrane, but rather that these interaction potentials be quasi-uniform there, which leads to negligible supplementary forces (proportional to the gradient of the potential) in the transport equations.

The simplifying assumption of quasi-equilibrium at the feed− and permeate−membrane interfaces allows the ionic concentrations within the membrane to be approximately related to the external concentrations via a quasi-equilibrium partition coefficient. In general, the ionic partition coefficient for ion *i* in the mixture can be factored into various contributions originating from the different physicochemical interactions operating between the ions in solution (bulk or intrapore) and between the ions in the pores and the membrane matrix

k_i = [electrostatic (Donnan)] × (steric) × (dielectric) × [solvation (Born)] × ...

We note that including the supplementary interactions (other than electrostatic) in ion partitioning across the external solution−membrane interfaces is not incompatible with neglecting the supplementary forces they engender within the membrane core: In these interfacial regions, the interaction potentials associated with these supplementary interactions are strongly varying, which could give rise to nonnegligible interfacial forces. Although the above framework is capable of accounting for any number of contributions to ion partitioning, in illustrating our theoretical results below through specific examples, we limit ourselves to the HET model. (It should be kept in mind that there is still no consensus as to the relative importance of the different supplementary mechanisms currently being invoked as being responsible for ion rejection behavior in nanoporous membranes.)

It has been shown[15,17,19] that the homogeneous model is valid when $r_p/\lambda_m < 2$, where λ_m is a Debye length associated with the effective membrane charge density, $\lambda_m = (2\epsilon RT/|z_1|F^2|X_m|)^{1/2}$. These two relations lead to the following inequality that delimits the range of validity for the homogeneous approximation

$$|X_m| < \frac{1.5}{|z_1| r_p^{\,2}} \tag{12}$$

where r_p is in nanometers and X_m is in moles per liter. The domain of validity of the homogeneous model covers the NF and most of the tight ultrafiltration (UF) range.

3. HET Model: Determination of Partition Coefficients

In the case of the ENP model, the Donnan partition coefficients satisfy eq 9, and it is clear that these partition coefficients depend only on electrostatic effects (for the feed side, $\Delta\phi_D^f$). In the general HET model, we have

$$k_i^f = \frac{\bar{c}_i^f}{c_i^f} = (\gamma_i^f/\bar{\gamma}_i^f) \exp\left[-\frac{z_i F}{RT} \Delta\phi_D^f\right]$$

In the HET model, this general expression reduces to

$$k_i^f = \Phi_i^S \exp(-z_i \Delta\tilde{\phi}_D^f) \tag{13}$$

with $\Delta\tilde{\phi} = F\Delta\phi/RT$ the dimensionless electric potential, and therefore

$$k_2^f = \Phi_2^S \left(\frac{k_1^f}{\Phi_1^S}\right)^{-|z_2/z_1|}$$

[A similar relation holds on the permeate (p) side.]

Electroneutrality at the feed−membrane interface ($x = 0^+$) (eq 4) gives

$$k_1^f - k_2^f - \hat{\xi}_f = 0 \tag{14}$$

with

$$\hat{\xi}_f = \frac{|X_m|}{|z_1|\nu_1 c^f}$$

By introducing $\Gamma = \exp(-\Delta\tilde{\phi}_D^f)$, k_i^f can be put in the following form

$$k_i^{\mathrm{f}} = \Phi_i^{\mathrm{S}} \Gamma^{z_i} \tag{15}$$

Equation 14 then becomes a polynomial in Γ that depends on the ion valences (for which only one solution is physically valid)

$$\Phi_1^{\mathrm{S}} \Gamma^{z_1} - \Phi_2^{\mathrm{S}} \Gamma^{z_2} - \hat{\bar{\xi}}_{\mathrm{f}} = 0 \tag{16}$$

For a symmetric electrolyte ([z:z]), eq 14 is a quadratic equation whose solution is

$$\Gamma = \left[\frac{-\mathrm{sgn}(X_{\mathrm{m}}) \hat{\bar{\xi}}_{\mathrm{f}} + \sqrt{\hat{\bar{\xi}}_{\mathrm{f}}^2 + 4\Phi_1^{\mathrm{S}}\,\Phi_2^{\mathrm{S}}}}{2\Phi_{\mathrm{cation}}^{\mathrm{S}}} \right]^{1/z} \tag{17}$$

For asymmetric [1:2] or [2:1] salts, eq 16 becomes a third-order polynomial whose solution depends not only on the salt studied, but also on the sign of the membrane charge density. The solution of this third-order polynomial is $\Gamma^{\mathrm{f}} = \Gamma_{z_1:z_2}^{\mathrm{sgn}(X_{\mathrm{m}})}$ (feed side), where

$$\begin{aligned} \Gamma_{1:2}^{+} &= \Gamma_{\mathrm{asym}}(\Phi_{\mathrm{anion}}^{\mathrm{S}}, \Phi_{\mathrm{cation}}^{\mathrm{S}}, \hat{\bar{\xi}}_{\mathrm{f}}) \\ \Gamma_{2:1}^{+} &= [\Gamma_{\mathrm{asym}}(\Phi_{\mathrm{cation}}^{\mathrm{S}}, \Phi_{\mathrm{anion}}^{\mathrm{S}}, -\hat{\bar{\xi}}_{\mathrm{f}})]^{-1} \\ \Gamma_{1:2}^{-} &= [\Gamma_{\mathrm{asym}}(\Phi_{\mathrm{cation}}^{\mathrm{S}}, \Phi_{\mathrm{anion}}^{\mathrm{S}}, \hat{\bar{\xi}}_{\mathrm{f}})]^{-1} \\ \Gamma_{2:1}^{-} &= \Gamma_{\mathrm{asym}}(\Phi_{\mathrm{anion}}^{\mathrm{S}}, \Phi_{\mathrm{cation}}^{\mathrm{S}}, -\hat{\bar{\xi}}_{\mathrm{f}}) \end{aligned} \tag{18}$$

and

$$\Gamma_{\mathrm{asym}}(r,s,t) = \frac{1}{6} \frac{\Lambda^{1/3}}{s} - \frac{2t}{\Lambda^{1/3}} \tag{19}$$

is the physical solution of $s\Gamma^3 + t\Gamma - r = 0$ with

$$\Lambda(r,s,t) = 108rs^2 + 12\sqrt{3}\sqrt{s^3(4t^3 + 27r^2 s)}$$

The solution of eq 16 at the membrane−permeate interface can be obtained from eqs 18 by replacing the variable $\hat{\bar{\xi}}_{\mathrm{f}}$ by $\hat{\bar{\xi}}_{\mathrm{f}}/T$ with T the transmission rate ($T = 1 - R = c_i^{\mathrm{p}}/c_i^{\mathrm{f}}$). In eqs 18, the subscripts are the absolute values of the counterion and the co-ion valences, and the superscript is the sign of the membrane charge.

4. Rejection Rates

In steady-state nanofiltration, the electric current density vanishes

$$J_{\mathrm{c}} = F \sum_{i=1}^{2} z_i j_i = 0 \tag{20}$$

and the molar and volume fluxes are linked by the filtration condition

$$j_i = j_{\mathrm{v}} c_i^{\mathrm{p}} \tag{21}$$

which relates the permeate concentration to the ionic and volume flux densities crossing the membrane.

a. Classic Extended Nernst−Planck Equation. Equation 5, along with eqs 4 and 20, allows one to obtain a relation between the electric potential and the ionic concentrations $\bar{c}_i$

$$\partial_x \tilde{\phi} = -\frac{\sum_{i=1}^{2} z_i \bar{D}_i \partial_x \bar{c}_i + X_{\mathrm{m}} j_{\mathrm{v}}}{\sum_{i=1}^{2} z_i^2 \bar{c}_i \bar{D}_i} \tag{22}$$

Electroneutrality in the membrane (eq 4) leads to

$$\partial_x \bar{c}_1(x) = -\frac{z_2}{z_1} \partial_x \bar{c}_2(x) \tag{23}$$

if X_{m} is assumed constant inside the membrane.

By combining eqs 4, 5, and 20 with eq 23, we obtain the canonical form for the co-ion flux density

$$j_2 = -P_2(\bar{c}_2) \partial_x \bar{c}_2 + j_{\mathrm{v}} \bar{c}_2 [1 - \sigma_2(\bar{c}_2)] \tag{24}$$

with

$$-P_2(\bar{c}_2) = -\bar{D}_2 + \frac{(|z_2|\bar{c}_2 \bar{D}_2)\,[|z_2|(\bar{D}_2 - \bar{D}_1)]}{|z_2|\bar{c}_2\,(|z_1|\bar{D}_1 + |z_2|\bar{D}_2) + |z_1|\bar{D}_1|X_{\mathrm{m}}|}$$

$$1 - \sigma(\bar{c}_2) = 1 + \frac{|z_2|\bar{D}_2|X_{\mathrm{m}}|}{|z_2|\bar{c}_2(|z_1|\bar{D}_1 + |z_2|\bar{D}_2) + |z_1|\bar{D}_1|X_{\mathrm{m}}|}$$

where $P_2(\bar{c}_2)$ is the effective co-ion permeability coefficient (m^2/s) and $\sigma_2(\bar{c}_2)$ is the effective co-ion reflection coefficient.

Introducing $y_2 = \bar{c}_2(x)/c_2^{\mathrm{f}}$ into eqs 5 and 22 yields the following integral

$$Pe = \frac{j_{\mathrm{v}} l_{\mathrm{m}}}{\bar{D}_{\max}} = \frac{\bar{D}_{\mathrm{s}}}{\bar{D}_{\max}} \int_{k_2^{\mathrm{f}}}^{Tk_2^{\mathrm{p}}} \frac{y_2 + \alpha}{y_2^2 + b(T) y_2 + a(T)} dy_2 \tag{25}$$

with

$$Pe = \frac{j_{\mathrm{v}}}{K}$$

$$K = \frac{\bar{D}_{\max}}{l_{\mathrm{m}}}$$

$$\alpha = \frac{\hat{\bar{\xi}}_{\mathrm{f}}}{1 + \tau_{\mathrm{v}}} \quad \text{and} \quad \tau_{\mathrm{v}} = \frac{|z_2|}{|z_1|}$$

$$a(T) = -T\,\bar{t}_1 \hat{\bar{\xi}}_{\mathrm{f}}$$

$$b(T) = \hat{\bar{\xi}}_{\mathrm{f}} - T$$

where Pe is the dimensionless Peclet number; K is the mass-transfer coefficient ($\mathrm{m \cdot s^{-1}}$ or $\mathrm{L \cdot h^{-1} \cdot m^{-2}}$); and $\bar{D}_{\mathrm{s}}$ and $\bar{D}_{\max}$ are the salt and maximum ion diffusion coefficients in the membrane, respectively, with $\bar{D}_{\max} = \max(\bar{D}_1, \bar{D}_2)$ and

$$\bar{D}_{\mathrm{s}} = \frac{(|z_1| + |z_2|)\bar{D}_1 \bar{D}_2}{|z_1|\bar{D}_1 + |z_2|\bar{D}_2}$$

The choice of using $\bar{D}_{\max}$ in the definition of Pe allows this definition to be easily extended to multielectrolyte mixtures (for which a unique $\bar{D}_{\mathrm{s}}$ cannot be defined).

By performing the integral in eq 25, we obtain the following expression

$$Pe = \frac{\bar{D}_s}{2\bar{D}_{max}}\left(\ln\left[\frac{g(Tk_2^p)}{g(k_2^f)}\right] + \frac{\hat{\xi}_f\left(\frac{1-\tau_v}{1+\tau_v}\right)+T}{\sqrt{q(T)}}\ln\left\{\frac{[g'(Tk_2^p)-\sqrt{q(T)}][g'(k_2^f)+\sqrt{q(T)}]}{[g'(Tk_2^p)+\sqrt{q(T)}][g'(k_2^f)-\sqrt{q(T)}]}\right\}\right) \quad (26)$$

where g and g' are two functions defined as

$$g(x) = x^2 + b(T)x + a(T)$$

$$g'(x) = 2x + b(T)$$

and

$$q(T) = (\hat{\xi}_f)^2 + T^2 - 2T\hat{\xi}_f(1-2\bar{t}_1)$$

When combined with analytical expressions for the Donnan partition coefficients (k_2^f and k_2^p) for symmetric and asymmetric ([1:2] or [2:1]) salts,[15] eq 26 gives the rejection rate $R = 1 - T$ versus the volume flux in parametric form. In Figure 1, we compare the analytical results for NaCl rejection for a typical NF membrane with numerical calculations obtained using Nanoflux. As another check on our calculation, we use the expression for the high-flux limiting rejection (eq 59[15])

$$R_{lim} = 1 - \frac{k_2^f}{\bar{t}_1 + (1-\bar{t}_1)(k_2^f)^{1+(|z_1|/|z_2|)}}$$

where

$$\bar{t}_i = \frac{|z_i|\bar{D}_i}{|z_1|\bar{D}_1 + |z_2|\bar{D}_2}$$

is the intramembrane ionic transport number.

In Figure 1, the horizontal line, the curve, and the points represent the limiting rejection rate,[15] the exact analytical results (eq 26), and the Nanoflux calculations, respectively. There is excellent agreement between the Nanoflux calculations and the analytic results (eq 26), and the horizontal line representing R_{lim} is clearly the upper limit of rejection.

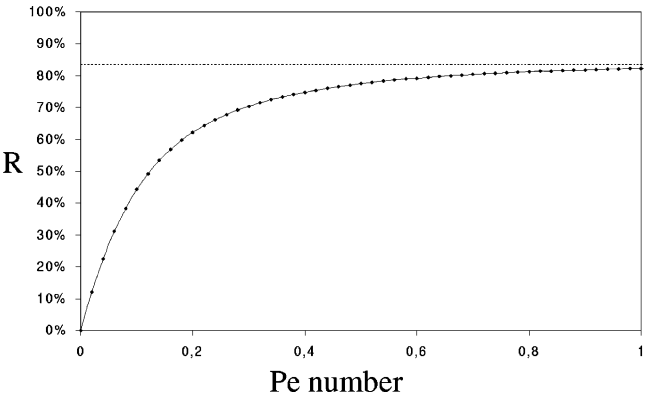

Figure 1. ENP model: R vs Péclet number for NaCl, with $c^f = 10^{-3}$ M and $X_m = 10^{-2}$ M.

b. Hindered Extended Nernst−Planck Model. Although, in the classic ENP model, particles are treated as pointlike, in the HET model, the choice of ion size presents additional difficulties. For the purposes of demonstration, we consider here, as a first approximation, the case in which the ion size obeys the Stokes−Einstein relation[24−26]

$$r_i^s = \frac{kT}{6\pi\eta D_i} \quad (27)$$

where r_i^s is the radius of the solute (m), k is the Boltzmann constant (1.38×10^{-23} J·K^{-1}), T is the temperature (K), and η is the dynamic viscosity ($= 1.0019 \times 10^{-3}$ Pa·s at 20 °C).

Ion transfer in biological channels and recent rejection measurements for ion mixtures using artificial nanofilters suggest, however, that the bare ion crystal (or Pauling) radius is most likely the appropriate choice (Table 1).[16,28]

TABLE 1: Bulk Diffusion Coefficients and Stokes−Einstein and Pauling Radii of the Four Ions Studied[a]

ion	bulk diffusion coefficient (m^2·s^{-1})	radius (nm)	
		Stokes−Einstein	Pauling
Na^+	1.334×10^{-9}	0.184	0.095
Ca^{2+}	0.792×10^{-9}	0.309	0.099
Cl^-	2.032×10^{-9}	0.121	0.181
SO_4^{2-}	1.065×10^{-9}	0.230	0.290

[a] $T = 25$ °C.

Within the framework of the HET model (eqs 4, 11, 20, and 21), we obtain the following relation between the electric potential and the ionic concentrations

$$\partial_x\tilde{\phi}(x) = \frac{\sum_{i=1}^{2}\{-z_i\bar{D}_i\partial_x\bar{c}_i(x) + j_v[z_iK_{i,c}\bar{c}_i(x)]\}}{\sum_{i=1}^{2}z_i^2\bar{D}_i\bar{c}_i(x)} \quad (28)$$

Following the method outlined in section 4a, we now solve eq 11 instead of eq 5 to obtain the canonical form (eq 24) with the same $P_2(\bar{c}_2)$ as in the ENP model, but now with

$$1 - \sigma(\bar{c}_2) = K_{2,c} + \frac{(|z_2|\bar{D}_2)[|z_2|\bar{c}_2(K_{1,c}-K_{2,c}) + K_{1,c}|X_m|]}{|z_2|\bar{c}_2(|z_1|\bar{D}_1 + |z_2|\bar{D}_2) + |z_1|\bar{D}_1|X_m|}$$

as one minus the co-ion reflection coefficient in the HET model.

Direct integration leads to an equation similar to eq 26

$$Pe = \frac{j_v l_m}{\bar{D}_{max}} = \frac{\bar{D}_s}{\bar{D}_{max}\omega}\int_{k_2^f}^{Tk_2^p}\frac{y_2+\alpha}{y_2^2+\beta(T)y_2+\gamma(T)}\,dy_2 \quad (29)$$

After carrying out the integration, we obtain

$$Pe = \frac{\bar{D}_s}{2\bar{D}_{max}\omega}\left(\ln\left[\frac{f(Tk_2^p)}{f(k_2^f)}\right] + \frac{\hat{\xi}_f\left(\frac{1-\tau_v}{1+\tau_v}\right)+\frac{T}{\omega}}{\sqrt{q(T)}}\ln\left\{\frac{[f'(Tk_2^p)-\sqrt{q(T)}][f'(k_2^f)+\sqrt{q(T)}]}{[f'(Tk_2^p)+\sqrt{q(T)}][f'(k_2^f)-\sqrt{q(T)}]}\right\}\right) \quad (30)$$

where

$$\omega = K_{2,c}\bar{t}_1 + K_{1,c}\bar{t}_2$$

$$q(T) = \hat{\xi}_f^2 + (T/\omega)^2 - (2T\hat{\xi}_f/\omega)(1 - 2\bar{t}_1)$$

$$\gamma(T) = -T\bar{t}_1\hat{\xi}_f/\omega$$

$$\beta(T) = \hat{\xi}_f - T/\omega$$

and f and f' are two functions defined by

$$f(x) = x^2 + \beta(T)x + \gamma(T)$$

and

$$f'(x) = 2x + \beta(T)$$

We note that the factors γ, β, and ω tend to a, b, and 1, respectively (cf. section 4a) when the ion size tends to zero. Indeed, in this limit, the hindrance factors $K_{i,c}$ and $K_{i,d}$ tend to 1, and eq 30 reduces to eq 26.

To obtain the limiting transmission rate at high Péclet number, we use eq 11, evaluated at $x = 0^+$ (a valid approach given the flatness of the concentration profiles in this limit), after having neglected the diffusive term

$$j_i \approx -z_i\bar{D}_i\bar{c}_i(0^+)\partial_x\tilde{\phi}(0^+) + K_{i,c}\bar{c}_i(0^+)j_v = c_i^p j_v \quad (31)$$

By combining this expression for the co-ion ($i = 2$), expression 28 for the electric potential without the gradient term, and electroneutrality at the feed−membrane interface ($x = 0^+$) (eq 4), we obtain an analytic expression for T_{lim}

$$T_{lim} = k_2^f\left[K_{2,c} + \bar{t}_2\frac{\sum_{i=1}^{2}(-1)^{i-1}K_{i,c}k_i^f}{\sum_{i=1}^{2}\bar{t}_i k_i^f}\right] \quad (32)$$

Using the normalized electroneutrality relation (eq 14), we can express eq 32 as a function of k_2^f only to find the limiting rejection

$$R_{lim} = 1 - k_2^f\left[K_{2,c} + \bar{t}_2\frac{k_2^f(K_{1,c} - K_{2,c}) + K_{1,c}|\hat{\xi}_f|}{k_2^f + \bar{t}_1|\hat{\xi}_f|}\right] \quad (33)$$

Figure 2 shows the excellent agreement between the analytical calculations (eq 30); the Nanoflux numerical calculations; and, for high Péclet number, the horizontal line representing R_{lim}.

We note for both Figures 1 and 2 that the limiting rejection is about 80%; the normalized charge density $\xi = X_m/c^f$ is, however, 2 times weaker in Figure 2 than in Figure 1 (+10 for Figure 1 but only +5 in Figure 2) for the same salt. The similarity between Figures 1 and 2 can be explained by the importance of steric effects in Figure 2, because the ratio $\lambda_i = r_i/r_p$ is not 0 in the HET model (as it is in the classic ENP model). Figure 3a−d shows the influence of hindered transport effects on ion rejection for a positively charged membrane within the scope of the HET model when r_p is equal to 1 nm and when the ionic size tends to zero under the same conditions for [1:1], [2:1], [1:2], and [2:2] salts. Figure 3a−d clearly shows that the choice of ion size (Stokes−Einstein, Pauling, or vanishing) can considerably influence ion rejection. As can be seen, this influence can be rather complex and will be treated in greater detail elsewhere. Suffice it to say here that, when the two ion rejection mechanisms incorporated into the HET model (electrostatic and steric) are both acting in concert (large co-ion and small counterion), the salt rejection is higher than when the two ion rejection mechanisms are acting in opposition (small co-ion and large counterion). This explains why, in Figure 3a−d, where the membrane charge density is positive, the Stokes−Einstein choice for ion size always give rise to higher rejections than the Pauling one. (Table 1 shows that the Stokes−Einstein choice leads to large cations, which are the co-ions here, and small anions and that the Pauling choice leads to small cations and large anions.) For [1:1], [1:2], and [2:2] salts (parts a, c, and d, respectively, of Figure 3), we also find, as expected intuitively, the lowest salt rejection when the ion size vanishes (ENP model). On the other hand, somewhat counterintuitively, the rejection of a salt with a large divalent counterion and small co-ion ([2:1] salt, HET Pauling model, Figure 3b) can be lower than that of the ENP model (vanishing ion size). Indeed, for such salts, we find that, if the normalized membrane charge density is sufficiently high, as it is here, then the limiting salt rejection *decreases* with decreasing pore radius (and can even become strongly negative for sufficiently small pore radius). The explanation for this anomalous behavior can once again be found in the competition between the two ion rejection mechanisms in the HET Pauling model: Although the positive membrane charge tends to strongly attract the divalent sulfate counterions, the steric repulsion is also strong because of the large counterion size.

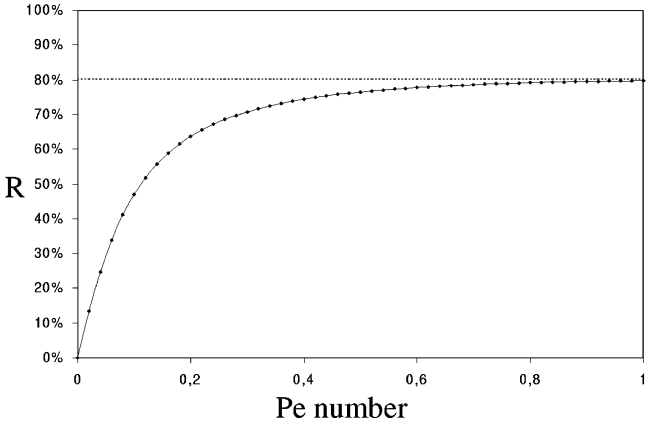

Figure 2. HET model: R vs Péclet number for NaCl, $c^f = 10^{-3}$ M and $X_m = 5 \times 10^{-3}$M and $r_p = 1$ nm.

5. Electric Potential

a. Classic Extended Nernst−Planck Equation. Equation 22 gives the gradient of the electric potential as a function of the position in the membrane (variable x). Using electroneutrality, it is possible to express this formula in terms of only one concentration (here, the concentration of the co-ion, $i = 2$). Using

$$\partial_x\tilde{\phi} = \partial_{y_2}\phi\cdot\partial_x y_2 \quad (34)$$

in eq 22 leads to

$$\partial_{y_2}\phi = \left(\frac{\bar{D}_1 - \bar{D}_2}{z_2\bar{D}_2 - z_1\bar{D}_1}\right)\left(\frac{1}{y_2 + \bar{t}_1\hat{\xi}_f}\right) + \beta\frac{y_2 + \alpha}{(y_2 + \bar{t}_1\hat{\xi}_f)[y_2^2 + b(T)y_2 + a(T)]} \quad (35)$$

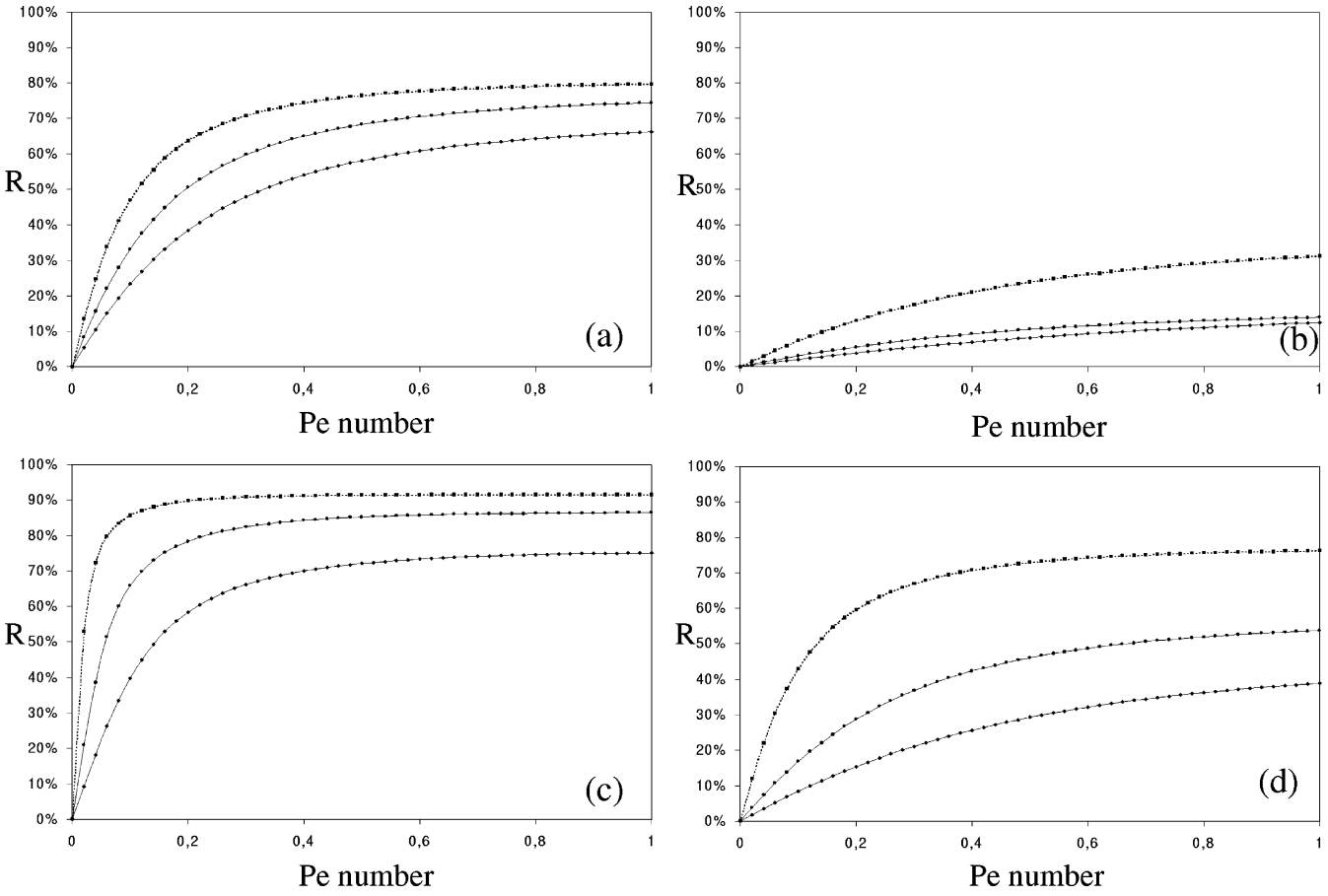

Figure 3. *R* vs Péclet number for (a) NaCl, (b) Na_2SO_4, (c) $CaCl_2$, and (d) $CaSO_4$ with $\xi = X_m/c^f = +5$ and $r_p = 1$ nm. For plots a, c, and d, the curves and points represent, in order of increasing rejection, the classic ENP, the HET Pauling, and the HET Stokes−Einstein models. For plot b, the curves and points represent, in order of increasing rejection, the HET Pauling, the classic ENP, and the HET Stokes−Einstein models.

with

$$\beta = -\frac{\hat{\bar{\xi}}_f \bar{D}_s}{|z_1|\bar{D}_1 + |z_2|\bar{D}_2}$$

Once integrated, eq 35 allows one to find the dimensionless electric potential in the membrane $\Delta\tilde{\phi}$

$$\Delta\tilde{\phi} = \tilde{\phi}(l_m^-) - \tilde{\phi}(0^+) = \Delta\tilde{\phi}_d + \Delta\tilde{\phi}_s \tag{36}$$

where

$$\Delta\tilde{\phi}_d = \frac{\bar{D}_1 - \bar{D}_2}{z_2\bar{D}_2 - z_1\bar{D}_1} \ln\left(\frac{Tk_2^p + \bar{t}_1\hat{\bar{\xi}}_f}{k_2^f + \bar{t}_1\hat{\bar{\xi}}_f}\right) \tag{37}$$

is the diffusion potential and

$$\Delta\tilde{\phi}_s = \beta\left(\frac{A}{2}\ln\left[\frac{g(Tk_2^p)}{g(k_2^f)}\right] + \frac{2B - Ab(T)}{2\sqrt{q(T)}}\ln\left\{\frac{[g'(Tk_2^p) - \sqrt{q(T)}][g'(k_2^f) + \sqrt{q(T)}]}{[g'(Tk_2^p) + \sqrt{q(T)}][g'(Tk_2^p) - \sqrt{q(T)}]}\right\} - A\ln\left(\frac{Tk_2^p + \bar{t}_1\hat{\bar{\xi}}_f}{k_2^f + \bar{t}_1\hat{\bar{\xi}}_f}\right)\right) \tag{38}$$

is the streaming potential with

$$A = [(1+\tau_v)\bar{t}_1\hat{\bar{\xi}}_f]^{-1}\left(1 - \frac{\bar{D}_1}{\bar{D}_2}\right)$$

and

$$B = [(1+\tau_v)\bar{t}_1\hat{\bar{\xi}}_f]^{-1}\left[\hat{\bar{\xi}}_f - T\left(1 - \frac{\bar{D}_1}{\bar{D}_2}\right)\right]$$

To obtain the (dimensionless) filtration potential $\Delta\tilde{\Phi}^F$, we first link the dimensionless Donnan potentials

$$\Delta\tilde{\phi}_D^f = -\frac{1}{z_2}\ln(k_2^f) \tag{39}$$

$$\Delta\tilde{\phi}_D^p = -\frac{1}{z_2}\ln(k_2^p) \tag{40}$$

to $\Delta\tilde{\phi}_d$ to obtain the membrane potential

$$\Delta\tilde{\phi}_m = -\Delta\tilde{\phi}_D^p + \Delta\tilde{\phi}_D^f + \Delta\tilde{\phi}_d \tag{41}$$

and finally incorporate the streaming potential

$$\Delta\tilde{\Phi}^F = \tilde{\Phi}^f - \tilde{\Phi}^p = -\Delta\tilde{\phi}_m - \Delta\tilde{\phi}_s \tag{42}$$

This definition of the filtration potential, $\Delta\tilde{\Phi}^F$, has been chosen

so that the sign of the membrane charge is the same as that of the electric potential. The analytical result for $\Delta\tilde{\Phi}^F$ is valid for any volume flux density. We can easily simplify this expression in certain limiting cases to find results already known in the literature. If, for instance, we assume that the volume flux tends to infinity, then eq 22 becomes

$$\partial_x\tilde{\phi} \approx -\frac{X_m j_v}{\sum_{i=1}^{2} z_i^2 \bar{D}_i \bar{c}_i(x)} \tag{43}$$

Because only the streaming potential, $\Delta\tilde{\phi}_s$, contributes to the filtration potential in this limit, it is then straightforward to find the following expression for the reduced streaming potential (ref 15, eq 66)

$$\nu_j \equiv \lim_{Pe\to\infty} \frac{d(\Delta\Phi^F)}{dj_v} = \frac{RT}{F}\left(\frac{X_m}{\nu_1|z_1|c^f}\right)\frac{l_m}{|z_1|\bar{D}_1 k_1^f + |z_2|\bar{D}_2 k_2^f} \tag{44}$$

In NF, it is more convenient to use ν_j to characterize the streaming potential, rather than the usual definition $\nu_P \equiv \lim_{\Delta P\to\infty} d(\Delta\Phi^F)/d(\Delta P)$, for two reasons: First, because electroviscous and osmotic effects complicate the relationship between j_v and ΔP (see section 6 below), ν_j is a more transparent NF membrane parameter. Second, because in composite systems, although thicker, larger pore supporting layers might contribute to the total pressure drop across the system (in a way that is often difficult to quantify), j_v is constant across the system in the steady state. The use of ν_j thus allows one to obtain a more direct link between membrane charge and structural parameters on one hand and measured electric potential on the other. The above result for ν_j in the ENP model will be used to check calculations performed within the HET model in the limit of zero ion size.

b. Hindered Extended Nernst−Planck Model. We have seen in eq 28 that the appearance of hindrance factors complicates the term containing the volume flux (cf. eq 22); thus the integration becomes more complex.

Using the same method as used in section 5a, we obtain, after some manipulation, an integrable expression

$$\partial_x\tilde{\phi} = (\partial_{y_2}\tilde{\phi}_d + \partial_{y_2}\tilde{\phi}_s)\partial_x y_2 \tag{45}$$

with

$$\partial_{y_2}\tilde{\phi}_d = \left(\frac{\bar{D}_1 - \bar{D}_2}{z_2\bar{D}_2 - z_1\bar{D}_1}\right)\left(\frac{1}{y_2 + \bar{t}_1\hat{\xi}_f}\right)$$

and

$$\partial_{y_2}\phi_s = \left(\frac{\delta y_2 - \epsilon}{y_2 + \bar{t}_1\hat{\xi}_f}\right)\left(\frac{y_2 + \alpha}{y_2^2 + \beta(T)y_2 + \gamma(T)}\right)$$

where

$$\delta = \frac{\bar{D}_s(K_c^+ - K_c^-)}{\omega(|z_1|\bar{D}_1 + |z_2|\bar{D}_2)}$$

with K_c^+ and K_c^- as the convective hindrance factors of the cation and the anion, respectively, and

$$\epsilon = \frac{K_{1,c}\hat{\xi}_f\bar{D}_s}{\omega(|z_1|\bar{D}_1 + |z_2|\bar{D}_2)}$$

In this way, we recover our previous expression for the diffusion potential, $\Delta\tilde{\phi}_d$ (eq 37), and find the HET version of the streaming potential

$$\Delta\tilde{\phi}_s = \frac{\bar{D}_s}{2\omega\sum_{i=1}^{2}|z_i|\bar{D}_i}\left(Y\ln\left[\frac{f(Tk_2^p)}{f(k_2^f)}\right] + \frac{2X - Y\beta(T)}{\sqrt{q(T)}}\ln\left\{\frac{[f'(Tk_2^p) - \sqrt{q(T)}][f'(k_2^f) + \sqrt{q(T)}]}{[f'(Tk_2^p) + \sqrt{q(T)}][f'(k_2^f) - \sqrt{q(T)}]}\right\}\right) + \frac{\bar{D}_s}{\omega\sum_{i=1}^{2}|z_i|\bar{D}_i}\left[(1+\tau_v)^{-1}\left(1 - \frac{\bar{D}_1}{\bar{D}_2}\right)\left(K_c^+ - K_c^- + \frac{K_{1,c}}{\bar{t}_1}\right)\right] \times \ln\left(\frac{Tk_2^p + \bar{t}_1\hat{\xi}_f}{k_2^f + \bar{t}_1\hat{\xi}_f}\right) \tag{46}$$

with

$$X = \frac{K_{1,c}}{\bar{t}_1(1+\tau_v)}\left[-\hat{\xi}_f + \frac{T}{\omega}\left(1 - \frac{\bar{D}_1}{\bar{D}_2}\right)\right] + \left[\frac{T}{\omega}\frac{(K_c^+ - K_c^-)}{1+\tau_v}\left(1 - \frac{\bar{D}_1}{\bar{D}_2}\right)\right]$$

and

$$Y = [(1+\tau_v)\bar{t}_1]^{-1}\left[(K_c^+ - K_c^- + K_{1,c})\frac{\bar{D}_1}{\bar{D}_2} - K_{1,c}\right]$$

As before (cf. section 5a, eq 36), the sum of the diffusion (eq 37) and streaming (eq 46) potentials represents only the membrane potential difference inside the membrane in the HET model. To obtain the total membrane potential difference, $\Delta\tilde{\phi}_m$, we have to join the Donnan potentials at the interfaces, which are obtained from eq 13

$$\Delta\tilde{\phi}_D^f = -\frac{1}{z_2}\ln\left(\frac{k_2^f}{\Phi_2^S}\right) \tag{47}$$

and

$$\Delta\tilde{\phi}_D^p = -\frac{1}{z_2}\ln\left(\frac{k_2^p}{\Phi_2^S}\right) \tag{48}$$

Using eqs 37 (diffusion potential), 46 (streaming potential), and 47 and 48 (Donnan potentials) in eqs 41 and 42, we obtain the filtration potential $\Delta\tilde{\Phi}^F$ within the HET model. In this model, the expression for the reduced streaming potential

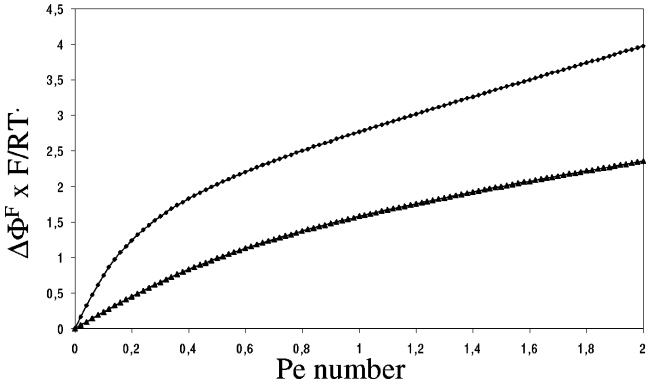

Figure 4. Filtration potential, $\Delta\tilde{\Phi}^{F}$ vs Péclet number for NaCl, with $c^{f} = 10^{-3}$ M and $X_m = 5 \times 10^{-3}$ M for the HET model (diamonds, $r_p = 1$ nm) and the classic ENP model (triangles).

contains a new term, which vanishes when the ion size tends to zero

$$\nu_j = \frac{RT}{F}\left[-\frac{\sum_{i=1}^{2} z_i K_{i,c}\bar{c}_i(0^+)}{\nu_1|z_1|c^f}\right]\frac{l_m}{|z_1|\bar{D}_1 k_1^f + |z_2|\bar{D}_2 k_2^f} \quad (49)$$

Equation 49 can also be written as follows

$$\nu_j = \frac{RT}{F}\left[1 - \frac{|z_2|\nu_2 k_2^f c^f (K_{2,c} - K_{1,c})}{K_{1,c}|X_m|}\right] \times \left(\frac{l_m}{|z_1|\bar{D}_1 k_1^f + |z_2|\bar{D}_2 k_2^f}\right)\left(\frac{K_{1,c}X_m}{\nu_1|z_1|c^f}\right) \quad (50)$$

We observe in Figure 4 the excellent agreement between the normalized filtration potential $\Delta\tilde{\Phi}^{F}$calculated numerically by Nanoflux and the analytical calculations. Furthermore, for high Péclet numbers, the slope of the analytical curve corresponds exactly to the reduced streaming potential (eq 50).

c. Comparison between the Classic ENP and HET Models. Equations 44 and 50 show that the reduced streaming potential depends on the salt feed concentration c^f, the membrane charge density X_m, the effective membrane thickness l_{eff}, and for the HET model, the ratio of the ion radius to the pore radius. For a given feed concentration and effective membrane charge and thickness, it is interesting to compare these models in order to quantify the relative importance of the hindered transport effects.

Equations 9 and 13 give the expressions for the partition coefficients within the scope of the classic ENP and the HET models (in this demonstration, we denote the two models using the superscripts I and II for the ENP and the HET models, respectively). We assume that the Donnan potential $\Delta\phi^f$ does not depend too much on the choice of model. Thus, the ratio between eqs 13 and 9 yields

$$\frac{k_i^{II,f}}{k_i^{I,f}} \approx \Phi_i^S \ (\leq 1) \quad (51)$$

and Figure A-1 (cf. the Appendix) shows that

$$K_{i,d} \leq 1 \quad \text{and} \quad \bar{D}_i^{II} \leq \bar{D}_i^{I} \quad (52)$$

we therefore find that

$$\left(\sum_i |z_i|\bar{D}_i^{II} k_i^{II,f}\right)^{-1} \geq \left(\sum_i |z_i|\bar{D}_i^{I} k_i^{I,f}\right)^{-1} \quad (53)$$

Because eq 51 implies that

$$\bar{c}_i^{II}(0^+) \approx \Phi_i^S \bar{c}_i^{I}(0^+) \quad (54)$$

we can combine eqs 49 and 54 to obtain

$$\nu_j^{II} = \frac{RT}{F}\left[-\frac{\sum_{i=1}^{2} z_i(K_{i,c}\Phi_i^S)\bar{c}_i^{I}(0^+)}{\nu_1|z_1|c^f}\right]\frac{l_m}{|z_1|\bar{D}_1 k_1^{II,f} + |z_2|\bar{D}_2 k_2^{II,f}} \quad (55)$$

Figure A-3 (cf. the Appendix) clearly shows that $K_{i,c}\Phi_i^S \leq 1$, which implies that

$$\sum_{i=1}^{2} z_i(K_{i,c}\Phi_i^S)\bar{c}_i^{I}(0^+) \leq \sum_{i=1}^{2} z_i\bar{c}_i^{I}(0^+) = -X_m \quad (56)$$

thus

$$-\sum_{i=1}^{2} z_i(K_{i,c}\Phi_i^S)\bar{c}_i^{I}(0^+) \geq X_m \quad (57)$$

Finally, we can conclude that

$$\nu_j(\text{HET}) \geq \nu_j(\text{ENP}) \quad (58)$$

and therefore

$$\Delta\Phi(\text{HET}) \geq \Delta\Phi(\text{ENP}) \quad (59)$$

Thus, for the same membrane charge density, the HET model gives rise to a larger filtration potential than the classic ENP model (see Figure 4).

6. Calculation of Volume Flux vs Transmembrane Pressure: Electroviscosity

a. Introduction. During the separation of salt solutions in nanofiltration, the membrane is electrically charged, with a sign that depends mainly on the feed solution pH and the electrolyte. The counterions are attracted into the pore, whereas the co-ions are repelled. Thus, if a pressure gradient is imposed, charge buildup occurs during a short transient period, and electroneutrality is not respected on a Debye length (λ_D). To reestablish macroscopic electroneutrality in the steady state, an electric force $q\vec{E}$ (derived from the streaming potential) is generated whose action on the counterions opposes that of the transmembrane pressure gradient (convective transport). If $X_m < 0$, this force makes the anions (co-ions) transfer more rapidly and the cations (counterions) more slowly. Figure 5 shows this phenomenon in the case of a negatively charged membrane.

Equations 37 and 38 for the ENP model and eqs 37−46 for the HET model allow one to obtain the electric potential difference in the membrane ($\Delta\tilde{\phi}$, eq 36) for any volume flux density. Using these results, it is possible to examine the effect of the electric potential on the transmembrane flux (electroviscous effect). Indeed, the volume-averaged Stokes equation in

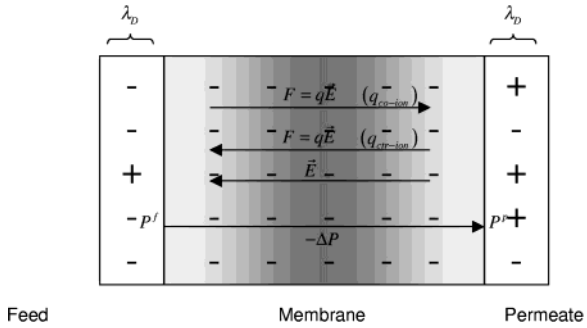

Figure 5. Schematic representation of electroviscous phenomenon.

the general HET model (cf. ref 22)

$$\frac{1}{L_p^0} j_v = -\partial_x P - \rho(x)\,\partial_x \phi - RT \sum_i \bar{c}_i(x)\,\partial_x(\ln \bar{\gamma}_i) \quad (60)$$

becomes, in the membrane ($0^+ < x < l_m^-$) sufficiently far from the interfacial regions

$$\frac{1}{L_p^0} j_v \approx -\partial_x P + RTX_m \partial_x \tilde{\phi} \quad (61)$$

[Here, $\rho(x) = F\Sigma_i z_i \bar{c}_i(x)$ is the local ion charge density.] We have once again assumed that supplementary body forces acting on the fluid in the membrane due to nonideality (last term in the averaged Stokes equation) are important only in the external solution−membrane interfacial regions (and thus negligible within the core of the membrane). Equation 61 is easily integrated to obtain the pressure difference in the membrane

$$\Delta P_m = P(l_m^-) - P(0^+) = -\frac{j_v l_m}{L_p^0} + RTX_m \Delta\tilde{\phi} \quad (62)$$

where L_p^0 is the pure-water permeability of the membrane ($L{\cdot}h^{-1}{\cdot}m^{-1}{\cdot}bar^{-1}$), $\Delta P_m = P(l^-) - P(0^+)$ is the pressure difference inside the membrane (bar), and $\Delta\tilde{\phi}$ is calculated using eqs 37 and 38 for the ENP model and eqs 37−46 for the HET model.

At the membrane−external solution interfaces, we have to account for osmotic pressure differences that arise because of ionic partitioning into the membrane. Indeed, we know that the total pressure difference is given by

$$\underline{\Delta} P = \underline{\Delta} P^f + \underline{\Delta} P_m + \underline{\Delta} P^p = P^f - P^p \quad (63)$$

with the following pressure jumps at the interfaces

$$\underline{\Delta} P^f = P^f - P(0^+)$$

$$\underline{\Delta} P^p = P(l_m^-) - P^p$$

where we have used the notation $\underline{\Delta} Q = -\Delta Q$ for any quantity Q.

By integrating the Stokes equation (eq 61) without the volume flux terms across the membrane−external solution interfaces (justified because of approximate mechanical equilibrium[22]) and combining this result with the quasicontinuity of the electrochemical potentials (eq 7), we obtain

$$\underline{\Delta} P^{f(p)} = \underline{\Delta}\pi^{f(p)}$$

where $\underline{\Delta}\pi^f = \Pi^f - \Pi(0^+)$ and $\underline{\Delta}\pi^p = \Pi(l_m^-) - \Pi^p$ are the interfacial osmotic pressure jumps and $\Pi(x) = RT\Sigma_i \bar{c}_i(x)$ is the local osmotic pressure.

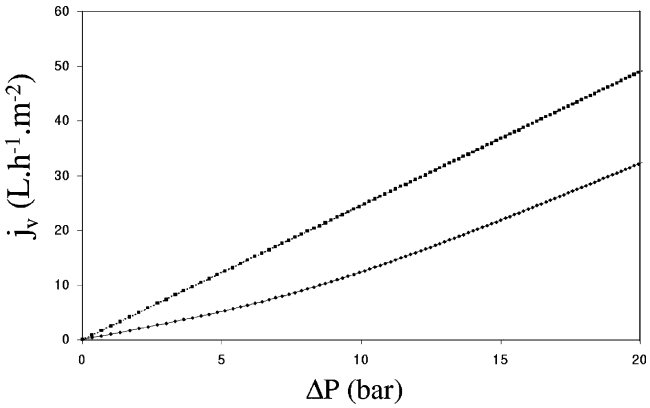

Figure 6. j_v vs ΔP for $MgCl_2$ at 10^{-1} M[29] and $X_m = 0.28$ M for a γ-alumina membrane, $L_p^0/l_m = 2.45$ L·h^{-1}·m^{-2}·bar^{-1}, with $K = 165.52$ L·h^{-1}·m^{-2} ($l_{eff} = 33.14$ μm). (Calculations performed with the classic ENP model. The upper curve is for pure water; the lower one for the salt solution.)

Combining the above results, we obtain an equation for the transmembrane pressure difference as a function of the volume flux density j_v

$$\frac{l_m}{L_p^0} j_v(1+\kappa) = \underline{\Delta} P - \underline{\Delta}\Pi\left(1 - \frac{k_2^f - Tk_2^p}{1-T}\right) + RTX_m[\Delta\tilde{\phi}_d + \Delta\tilde{\phi}_s - (\partial_x\tilde{\phi}_s)_{0^+} l_m] \quad (64)$$

which can also be written in standard form

$$j_v = \frac{L_p^0}{(1+\kappa) l_m}(\underline{\Delta} P - \Sigma\underline{\Delta}\Pi) \quad (65)$$

using $\underline{\Delta}\Pi = \Pi^f - \Pi^p$, the total osmotic pressure difference across the membrane; $\kappa = -RTL_p^0 X_m(\partial_x\tilde{\phi}_s)_{0^+} j_v^{-1}$, the electroviscosity coefficient (independent of j_v); and

$$\Sigma = 1 - \frac{k_2^f - Tk_2^p}{1-T} - \frac{X_m[\Delta\tilde{\phi}_d + \Delta\tilde{\phi}_s - (\partial_x\tilde{\phi}_s)_{0^+} l_m]}{c^f(\nu_1+\nu_2)(1-T)}$$

the global osmotic reflection coefficient, which, although j_v-dependent, tends to a constant value at high volume flux density.

Within the ENP model, we can rewrite the electroviscosity coefficient as

$$\kappa^{ENP} = \frac{RTL_p^0 X_m^2}{\sum_i z_i^2 \bar{D}_i \bar{c}_i(0^+)} = \frac{RTL_p^0 X_m^2}{c^f \nu_1 |z_1| \sum_i |z_i| \bar{D}_i k_i^f} \quad (66)$$

Within the HET model, we find

$$\kappa^{HET} = RTL_p^0 |X_m| \frac{\sum_{i=1}^{2} (-1)^{i+1} K_{i,c} k_i^f}{\sum_{i=1}^{2} |z_i| \bar{D}_i k_i^f} \quad (67)$$

Figure 6 shows the volume flux density vs pressure behavior of a $MgCl_2$ solution. The membrane charge density X_m and the mass-transfer coefficient K [$K = (K_{d,max} D_{max})/l_{eff}$] were adjusted

to account for the experimental salt rejection obtained using an alumina NF membrane.[29] The volume flux density curve, j_v vs ΔP, was calculated using eq 65. When the volume flux density increases, the curve becomes parallel to a straight line with slope

$$\lim_{Pe\to\infty} \frac{dj_v}{d\underline{\Delta}P} = \frac{L_p^0}{(1+\kappa)l_m} = \frac{K_D^0}{\eta^{eff}}\frac{1}{l_m} \tag{68}$$

where

$$\eta^{eff} = \eta^0(1+\kappa) \geq \eta^0 \tag{69}$$

and K_D^0 is the Darcy hydraulic permeability (m^2) ($L_p^0 = K_D^0/\eta^0$).

The upper straight lines in Figures 6−8 represent the volume flux density for pure water

$$j_v^w = L_p^0\frac{\underline{\Delta}P}{l_m} = \frac{K_D^0}{\eta^0}\frac{\underline{\Delta}P}{l_m} \tag{70}$$

and has the slope

$$\frac{j_v^w}{\underline{\Delta}P} = \frac{K_D^0}{\eta^0 l_m} \geq \frac{dj_v}{d\underline{\Delta}P} \tag{71}$$

The quantity η^{eff} represents the effective electroviscosity, because the salt−membrane system responds as if the viscosity of the fluid were greater than the pure water value.[9] On one hand, when the density of membrane charge squared increases slower than the salt feed concentration [$X_m \propto (c^f)^a$, $a < 1/2$], κ and therefore electroviscosity effects decrease as the salt feed concentration increases. On the other hand, if X_m increases with the concentration rapidly enough ($a > 1/2$), then electroviscosity effects increase with the salt feed concentration.

We note that the volume flux density of the solution studied in Figure 6 is very different from that of pure water (∼30% decrease at high pressure). This difference in flux density is quite important in this case because neither $\kappa = 0.51$ ($\eta^{eff}/\eta^0 = 1.51$) nor $\Sigma\Delta\Pi \approx 4.4$ bar is negligible ($\Sigma\Delta\Pi$ is high because of the high feed concentration and moderately high salt rejection). The term $\Sigma\Delta\Pi$ represents the x intercept of the straight line to which the volume flux density curve, j_v vs ΔP, tends asymptotically (with a slope $dj_v/d\Delta P$ that depends on the value of κ). The magnitude of the electroviscous and osmotic effects can clearly be sufficiently large for them to be important in predicting the productivity of industrial NF plants during a dimensioning study.

Figure 7 shows a comparison between the HET model ($\eta^{eff}/\eta^0 = 1.14$ and $\Sigma\Lambda\Pi \approx 0.042$ bar) and the classic ENP model ($\eta^{eff}/\eta^0 = 1.05$ and $\Sigma\Lambda\Pi \approx 0.03$ bar) for the same salt (10^{-3} M $CaSO_4$) under the same conditions. Figure 7 shows that, on one hand, the analytical and Nanoflux numerical calculations are in excellent agreement and, on the other hand, the gap between the saline solution and the pure water permeability is larger in the HET model than in the classic ENP one. This phenomenon can be explained by the calculations carried out in section 5c. Indeed, for the same membrane charge density, the inequality $\nu_j(\text{HET}) \geq \nu_j(\text{ENP})$ implies that $\kappa(\text{HET}) \geq \kappa(\text{ENP})$. Moreover, we know that $R^{HET} \geq R^{ENP}$, which implies that $\Delta\Pi^{HET} \geq \Delta\Pi^{ENP}$and $\Sigma^{HET} \geq \Sigma^{ENP}$. We can conclude that $(\Sigma\Delta\Pi)^{HET} \geq (\Sigma\Delta\Pi)^{ENP}$. Thus, as is observed in Figure 7, $j_v(\text{HET}) \leq j_v(\text{ENP})$ for the same transmembrane pressure.

Figure 8 represents the volume flux as a function of the transmembrane pressure for the same membrane and salt solution (10^{-3} M $CaSO_4$) as studied in Figure 7. The upper straight line is the pure-water permeability (I). The intermediate curve (II) was obtained using a simple reverse osmosis (RO) model for which $\Sigma = 1$ and $\kappa = 0$ in eq 65. The lower curve (III) represents the analytical solution (eq 65) for $r_p = 1$ nm (HET model). In this last case, $\eta^{eff}/\eta^0 \approx 1.14$, which implies that the permeability of the saline solution is about 14% weaker than that of pure water. We note that curve II is nearly superposed on curve I, because the electroviscosity effect is not taken into account in the simple RO model and, in this example, $\Sigma\Delta\Pi$ is practically negligible. Figure 8 clearly shows that this simple RO model is not generally appropriate for NF, as electroviscous effects can be important.

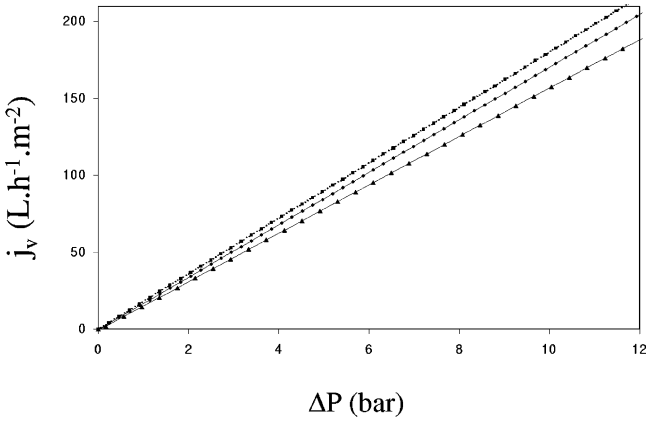

Figure 7. j_v vs ΔP for $CaSO_4$ with $c^f = 10^{-3}$ M, $X_m = 10^{-2}$ M, $L_p^0/l_m = 18$ L·h^{-1}·m^{-2}·bar^{-1}, and $l_{eff} = 100$ μm for (lower curve) the HET model ($r_p = 1$ nm), (intermediate) the ENP model ($r_i = 0$), and (upper) pure water. Points, Nanoflux calculations; curves, analytical calculations.

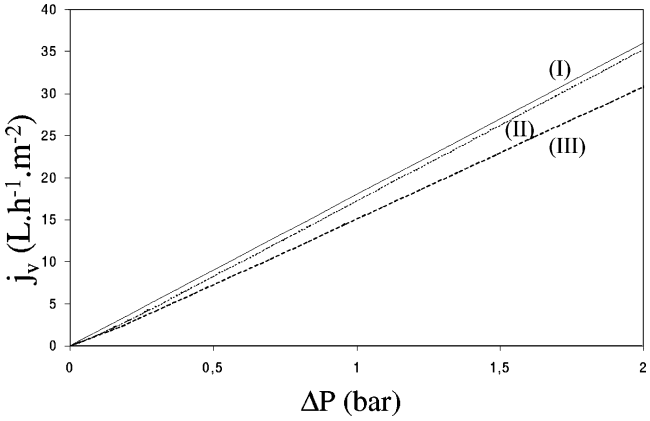

Figure 8. j_v vs ΔP for (I) pure water, $CaSO_4$, $c^f = 10^{-3}$M, $X_m = 10^{-2}$ M, $L_p^0/l_m = 18$ L·h^{-1}·m^{-2}·bar^{-1}, $l_{eff} = 100$ μm; (II) a simple RO model; and (III) the HET model ($r_p = 1$ nm).

7. Application of HET Model to a Tight UF Membrane

For a given membrane and given operating conditions, a coherent transport model should be able to account simultaneously for ion rejection (Figures 1−3), filtration potential (Figure 4), and volume flux density (Figures 6−8), using a unique choice for the membrane pore size, charge density, and effective thickness.

As a preliminary application of the model, we study a positively charged polylysine-cross-linked collodion membrane for which there are full rejection and streaming potential data at two feed concentrations;[30,31] unfortunately, even today, it is difficult to find a complete published data set (rejection, electric potential, flux density) for NF and tight UF membranes.[32−39]

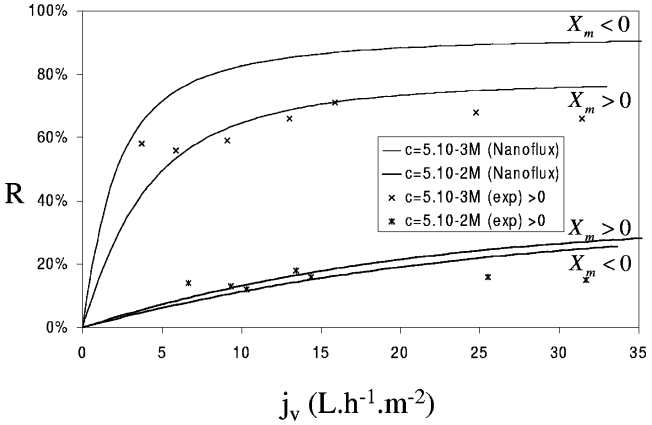

Figure 9. R vs j_v for KCl at 5×10^{-3} and 5×10^{-2} M for positively (experimental points and theoretical curves) and negatively (simulations) charged tight UF membranes[30,31] ($r_p \approx 3$ nm).

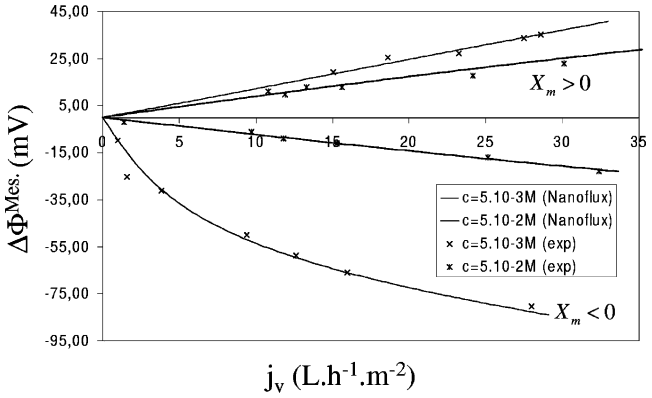

Figure 10. Experimental points and theoretical curves. $\Delta\Phi^{mes}$ vs j_v for KCl at 5×10^{-3} and $5 \times 10^{-2}M$ for positively and negatively charged tight UF membranes[30,31] ($r_p \approx 3$ nm).

In Figures 9 and 10, we present the experimental rejection and electric potential for this membrane as a function of volume flux density for KCl at feed concentrations of 5×10^{-2} and 5×10^{-3} M. The electric potential measurements include the Nernst (electrode) potential for anion reversible electrodes

$$\Delta\Phi^{mes} = \Delta\Phi^{F} + \frac{RT}{F}\ln\left(\frac{c^{p}_{Cl-}}{c^{f}_{Cl-}}\right)$$

The curves in these figures were obtained using the HET model with an estimated pore radius of 3 nm[31] and the following choice of effective membrane charge density and effective thickness

$$X_m = +3.75 \times 10^{-2}\ \text{M and } l_{eff} = 284.5\ \mu\text{m} \quad \text{for } c^f = 5 \times 10^{-3}\ \text{M}$$

$$X_m = 0.1\ \text{M and } l_{eff} = 180\ \mu\text{m for } c^f = 5 \times 10^{-2}\ \text{M}$$

It is important to note that these values, which were obtained by fitting the model to both rejection and potential data, are physically reasonable for these older tight UF membranes (cf. measured values for actual thicknesses and analytical ion-exchange capacities for similar collodion/polyvinylamine membranes, Table 2 of ref 31). This choice of membrane parameters allows one to account simultaneously for both ion rejection and filtration potential data. This is direct evidence for the global coherence of the model and indirect evidence that the active layer controls both rejection and potential; therefore, the contribution of any supporting layers, if there are any, appears

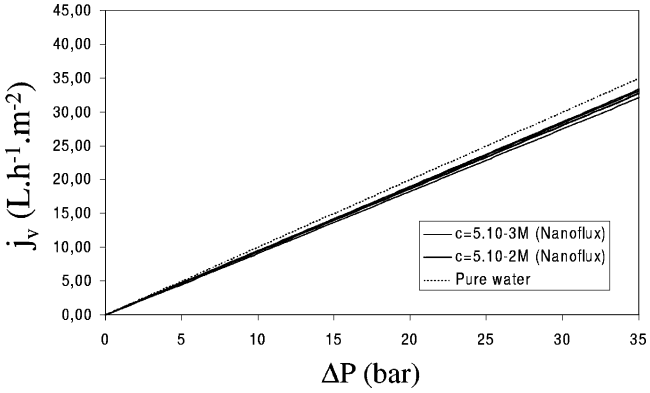

Figure 11. j_v vs ΔP simulations for KCl at 5×10^{-3} and 5×10^{-2} M for positively and negatively charged tight UF membranes[30,31] ($r_p \approx 3$ nm).

to be negligible (cf. ref 39). (The slight drop in rejection at high flux density is probably due to incipient concentration polarization effects not taken into account in the model.) As is usually the case, we observe that the salt rejection strongly decreases with increasing concentration, even though the effective membrane charge density itself increases; this is because X_m increases more slowly than the salt feed concentration [$X_m \propto (c^f)^a$, $a < 1$], and therefore the normalized effective membrane charge density, $\xi_f = X_m/c^f$, which directly controls the rejection amplitude, decreases with increasing concentration.

We have allowed the effective membrane thickness to depend on the salt concentration, because we believe that the effective tortuosity might include electrical effects that would tend to increase the effective thickness at low concentrations, where such effects are most important.[16,40] We do indeed observe that l_{eff} increases by a factor of 1.6 when the salt concentration decreases by a factor of 10. Although the experimental data for the flux density as a function of applied pressure were not published, we still plot in Figure 11 the model curves using the estimated value of 1 L·h^{-1}·m^{-2}·bar^{-1} for L_p^0/l_m; we observe that, under these conditions, both osmotic pressure and electroviscous effects appear to be rather weak.

Although negatively charged polylysine membranes were also obtained by succinylation of the positively charged ones, only the filtration potential data were published in refs 30 and 31. In this case, we first fit the model to the measured potential vs volume flux density data (Figure 10) to find

$$X_m = -0.1\ \text{M and } l_{eff} = 198.9\ \mu\text{m for } c^f = 5 \times 10^{-3}\ \text{M}$$

$$X_m = -0.1\ \text{M and } l_{eff} = 149.6\mu m \text{ for } c^f = 5 \times 10^{-2}\ \text{M}$$

and then used these membrane parameters to simulate the rejection and flux density (Figures 9 and 11). Contrary to what was found for the positively charged membrane, we found in this case that the effective negative membrane charge density remains approximately the same for the two salt concentrations studied, although, as before, l_{eff} does decrease with increasing concentration. We observe once again a strong drop in salt rejection (here only by simulation) with increasing salt concentration. At low salt concentration ($c^f = 5 \times 10^{-3}$ M, see Figure 9), we see that, by plotting the measured potential, $\Delta\Phi^{mes}$ (which includes the electrode potential), the curved part of the $\Delta\Phi^F$ vs j_v curve (see Figure 4) gets subtracted out for positive membrane charges and amplified for negative ones. The explanation is as follows: At low concentration, the strong co-ion exclusion, and therefore high salt rejection, leads to a

situation in which the low-flux nonlinear part of the $\Delta\Phi^F$ curve is dominated by the Donnan potential, which becomes equal in sign and amplitude to the electrode potential for negative membrane charge, leading to amplification, and opposite in sign but equal in amplitude to the electrode potential for positive membrane charge, leading to cancellation.

For both types of membranes studied, we can verify that inequality 12 is obeyed and, therefore, the homogeneous approximation to the SCM should be valid.

8. Conclusions

The purpose of this work was to calculate nanofiltration physical parameters by analytically solving the electrotransport equations. We have seen that this seems possible only in the case of simple saline solutions. These methods cannot therefore be used in real industrial situations where one often encounters up to 10 different species. Nonetheless, this work has allowed us to gain deeper insight into NF transport mechanisms via explicit analytical solutions to the transport equations. We have also been able to compare the nanofiltration parameters obtained using two different models. Our results confirm that ion and pore size cannot be neglected in the NF range and that size exclusion might be incorrectly estimated using the Stokes−Einstein choice of ionic radius instead of the crystal one.[16,40] We have also shown that electroviscous effects can be strong in NF. Furthermore, the sensitive dependence of the electroviscosity on the effective intramembrane ion diffusion coefficients explains why the electroviscous effect is amplified by both the hindered transport coefficients (finite pore and ion size) and tortuosity (large effective membrane thickness). Furthermore, the exact analytical results presented here for salt rejection, filtration potential, and volume flux density show clearly that the HET model is a true three-parameter model, and therefore, all three parameters (the membrane charge density, X_m; the effective membrane thickness, l_{eff}; and the membrane pore radius, r_p) must be specified before the model can be solved.

The preliminary application presented here is encouraging and suggests that the HET model provides a reasonably coherent description of ion transport in tight UF membranes. To perform more stringent tests of the model, it is necessary to obtain a full set of data, ideally as a function of feed salt concentration and pH, for the tighter NF membranes.

The excellent agreement between the Nanoflux numerical calculations and the analytical results for all of the parameters studied (rejection, electric potential, and flux density) has also allowed us to validate our numerical algorithm. We can therefore use Nanoflux with confidence for complex industrial problems. Because of adjustable parameters (X_m and l_{eff}) of the computer simulation program Nanoflux, we can build a database characteristic of salt/membrane pairs that can then be used to predict the behavior of complex salt mixtures.[16,40] Our goal is to predict NF performance in industrial situations such as effluent treatment and drinking water production. The use of Nanoflux should allow one to substantially reduce the time spent performing costly pilot tests, which should, in turn, lead to a more widespread use of nanofiltration in industry. Furthermore, the analytical analysis presented here should be useful in tackling one of the major open problems in the area of ion transport and partitioning in nanoporous media, namely, the role and importance of the supplementary interactions (besides the electrostatic one).

In a subsequent article, the analytical approach presented here will be used as the starting point for deriving simpler approximate expressions, valid in certain limiting cases, for all physical NF parameters.

Appendix

Analytic Determination of the Diffusive and Convective Hindrance Factors.[27]

$$K_{i,d} = \frac{6\pi}{K_t(\lambda_i)} \quad \text{and} \quad K_{i,c} = \frac{(2 - \Phi_i^S)K_s(\lambda_i)}{2K_t}$$

Calculation of K_t and K_s.

$$K_t(\lambda) = \frac{9}{4}\pi^2\sqrt{2}(1-\lambda)^{-5/2}\left[1 + \sum_{n=1}^{2} a_n(1-\lambda)^n\right] + \sum_{n=0}^{4} a_{n+3}\lambda^n$$

and

$$K_s(\lambda) = \frac{9}{4}\pi^2\sqrt{2}(1-\lambda)^{-5/2}\left[1 + \sum_{n=1}^{2} b_n(1-\lambda)^n\right] + \sum_{n=0}^{4} b_{n+3}\lambda^n$$

with $a_1 = -73/60$, $a_2 = 77.293/50.4$, $a_3 = -22.5083$, $a_4 = -5.6117$, $a_5 = -0.3363$, $a_6 = -1.216$, $a_7 = 1.647$, $b_1 = 7/60$, $b_2 = -2.227/50.4$, $b_3 = 4.018$, $b_4 = -3.9788$, $b_5 = -1.9215$, $b_6 = 4.392$, and $b_7 = 5.006$.

Study of Useful Functions Introduced in Section 2 and Used in Section 5c Demonstrations. Figures A-1−A-3 display plots of functions discussed in sections 2 and 5c.

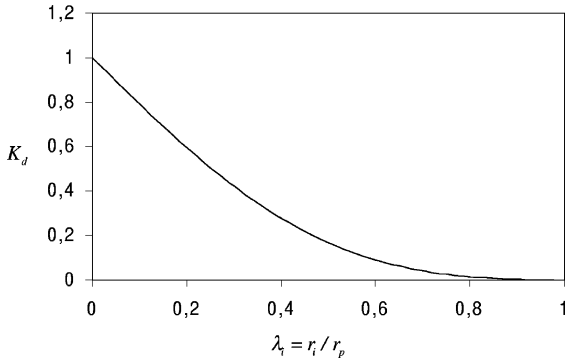

Figure A-1. K_d vs λ_i.

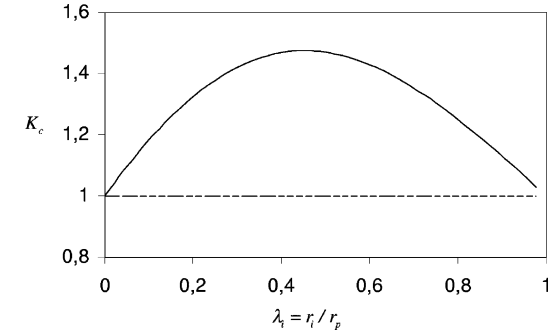

Figure A-2. K_c vs λ_i.

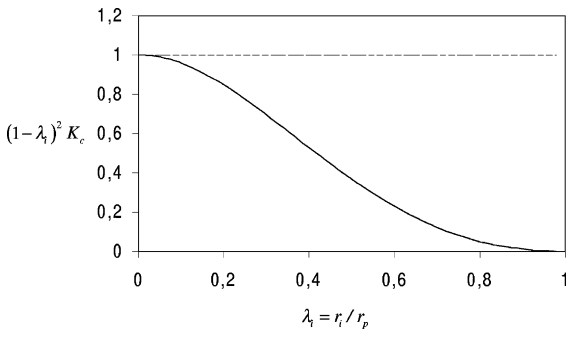

Figure A-3. $(1 - \lambda_i)^2 K_c$ vs λ_i.

References and Notes

(1) Petersen, R. *J. Membr. Sci.* **1993**, *83*, 81.
(2) Eriksson, P. *Environ. Prog.* **1988**, *7*, 58.
(3) Raman, L. P.; Cheryan, M.; Rajagopalan, N. *Chem. Eng. Prog.* **1994**, *90*, 68.
(4) Jacazio, G.; Probstein, R. F.; Sonin, A. A.; Yung, D. *J. Phys. Chem.* **1972**, *76*, 4015.
(5) Dresner, L. *J. Phys. Chem.* **1965**, *69*, 2230.
(6) Dresner, L. *Desalination* **1972**, *10*, 27.
(7) Dresner, L. *J. Phys. Chem.* **1972**, *76*, 2256.
(8) Dresner, L.; Kraus, K. A. *J. Phys. Chem.* **1963**, *67*, 990.
(9) Neogi, P.; Ruckenstein, E. *J. Colloid Interface Sci.* **1981**, *79*, 159.
(10) Cervera, J.; Garcia-Morales, V.; Pellicer, J. *J. Phys. Chem. B* **2003**, *107*, 8300.
(11) Schuss, Z.; Nadler, B.; Eisenberg, R. S. *Phys. Rev. E* **2001**, *64*.
(12) Graf, P.; Kurnikova, M. G.; Coalson, R. D.; Nitzan, A. *J. Phys. Chem. B* **2004**, *108*, 2006.
(13) Tsuru, T.; Nakao, S.; Kimura, S. *J. Chem. Eng. Jpn.* **1991**, *24*, 511.
(14) Tsuru, T.; Urairi, M.; Nakao, S.; Kimura, S. *J. Chem. Eng. Jpn.* **1991**, 518.
(15) Palmeri, J.; Blanc, P.; Larbot, A.; David, P. *J. Membr. Sci.* **1999**, *160*, 141.
(16) Palmeri, J.; Sandeaux, J.; Sandeaux, R.; Lefebvre, X.; David, P.; Guizard, C.; Amblard, P.; Diaz, J.-F.; Lamaze, B. *Desalination* **2002**, *147*, 231.
(17) Cwirko, E. H.; Carbonell, R. *J. Colloid Interface Sci.***1989**, *129*, 513.
(18) Yaroshchuk, A. E. *Adv. Colloid Interface Sci.* **1995**, *60*, 1.
(19) Wang, X.-L.; Tsuru, T.; Nakao, S.; Kimura, S. *J. Membr. Sci.* **1995**, *103*, 117.
(20) Schlögl, R. *Ber. Bunsen-Ges. Phys. Chem.* **1966**, *70*, 400.
(21) Hoffer, E.; Kedem, O. *Desalination* **1967**, *2*, 25.
(22) Sonin, A. A. Osmosis and ion transport in charged porous membranes: macroscopic mechanistic model. In *Charged Gels and Membranes*; Sélégny, E., Ed.; Reidel: Dordrecht, The Netherlands, 1976; Vol. 1, p 255.
(23) Papet, S. Etude de la Synthèse de Matériaux Inorganiques en Milieu CO_2 Supercritique. Application à l'élaboration de Membranes Minérales de Filtration Tangentielle. Ph.D. Thesis, University of Montpellier II, Montpellier, France, 2000.
(24) Deen, W. M.; Satvat, B.; Jamieson, J. M. *Am. J. Physiol.* **1980**, *238*, F126.
(25) Wang, X.-L.; Tsuru, T.; Togoh, M.; Nakao, S.; Kimura, S. *J. Chem. Eng. Jpn.* **1995**, *28*, 372.
(26) Bowen, W. R.; Mukthar, H. *J. Membr. Sci.* **1996**, *112*, 263.
(27) Deen, W. M. *AIChE J.* **1987**, *33*, 1409.
(28) Hille, B. *Ionic Channels of Excitable Membrane*, 3rd ed.; Sinauer Associates Inc.: Sunderland, MA, 2001.
(29) Rios, G.; Joulie, R.; Sarrade, S.; Carlès, M. *AIChE J.* **1996**, *42*, 2521.
(30) Tanny, G.; Hoffer, E.; Kedem, O. Streaming potentials during hyperfiltration. In *Biological Aspects of Electrochemistry*; Milazzo, G., Ed.; Birkhauser Verlag: Basel, Switzerland, 1971; p 619 [*Experentia Suppl.* **1971**, *18*, 619].
(31) Tanny, G.; Kedem, O. *J. Colloid Interface Sci.***1975**, *51*, 177.
(32) Benavente, J.; Jonsson, G. *Colloids Surf. A: Physicochem. Eng. Aspects* **1999**, *159*, 431.
(33) Benavente, J.; Jonsson, G. *J. Membr. Sci.* **2000**, *172*, 189.
(34) Huisman, I. H.; Pradanos, P.; Hernandez, A. *J. Membr. Sci.* **2000**, *178*, 55.
(35) Condom, S.; Chemlal, S.; Chu, W.; Persin, M.; Larbot, A. *Sep. Purif. Technol.* **2001**, *25*, 545.
(36) Labbez, C.; Fievet, P.; Szymczyk, A.; Aoubiza, B.; Vidonne, A.; Pagetti, J. *J. Membr. Sci.* **2001**, *184*, 79.
(37) Pontié, M.; Chasseray, X.; Lemordant, D.; Lainé, J. M. *J. Membr. Sci.* **1997**, *129*, 126.
(38) El Marraki, Y.; Persin, M.; Sarrazin, J.; Cretin, M.; Larbot, A. *Sep. Purif. Technol.* **2001**, *25*, 493.
(39) Yaroshchuk, A. E.; Boiko, Y. P.; Makovetskiy, A. L. *Langmuir* **2002**, *18*, 5154.
(40) Lefebvre, X.; Palmeri, J.; Sandeaux, J.; Sandeaux, R.; David, P.; Maleyre, B.; Guizard, C.; Amblard, P.; Diaz, J.-F.; Lamaze, B. *Sep. Purif. Technol.* **2003**, *32*, 117.